Research Article | Vol. 30, No. 11 / 23 May 2022 / Optics Express 17754

Optics EXPRESS

Hybrid sensor based on a hollow square core fiber for temperature independent refractive index detection

DIANA PEREIRA,[1] JÖRG BIERLICH,[2] JENS KOBELKE,[2] AND MARTA S. FERREIRA[1,*]

[1] *i3N & Physics Department, University of Aveiro, Campus de Santiago, 3810-193 Aveiro, Portugal*
[2] *Leibniz Institute of Photonic Technology, Albert-Einstein-Str. 9, 07745 Jena, Germany*
[*] *marta.ferreira@ua.pt*

Abstract: In this work, a hybrid sensor based on a section of hollow square core fiber (HSCF) spliced between two single mode fibers is proposed for the measurement of refractive index of liquids. The sensor, with a length of a few millimeters, operates in a transmission configuration. Due to the HSCF inner geometry, two different interferometers are generated. The first, a Mach-Zehnder interferometer, is insensitive to the external refractive index, and presents a sensitivity to temperature of (29.2 ± 1.1) pm/°C. The second one, a cladding modal interferometer, is highly sensitive to the external refractive index. An experimental resolution of 1.0×10^{-4} was achieved for this component. Due to the different responses of each interferometer to the parameters under study, a compensation method was developed to attain refractive index measurements that are temperature independent. The proposed sensor can find applications in areas where refractive index measurements are required and the control of room temperature is a challenge, such as in the food and beverage industry, as well as in biochemical or biomedical industries.

1. Introduction

The detection of glucose with high reliability and accuracy is of great importance for many fields, such as in biomedicine, biochemistry, pharmaceutics, cosmetics, and food industry [1,2]. Usually, chemical analytical methods are employed to detect and quantify the glucose concentration in a sample. These techniques can require time consuming sample preparation steps, or rely on specific enzymes, which can have stability issues [2].

As the concentration of glucose in an aqueous solution is correlated with its refractive index, this parameter can also be used as a measurand. Optical fiber sensors can be an alternative to conventional refractometers due to their attractive characteristics, namely, immunity to electromagnetic interference, reduced dimensions and lightweight, high resolution and sensitivity, and the capability of being implemented in adverse environments [3].

A myriad of configurations has been proposed in the literature for the measurement of refractive index with optical fiber sensors [4]. For instance, fiber gratings [5,6], Fabry-Perot [7], Michelson [8], Mach-Zehnder [9], multimode interferometers [10,11], or even fiber loop mirrors [12] have been reported. To enhance the sensor sensitivity, usually the fiber diameter is reduced through chemical etching, which besides being a dangerous procedure, increases the fragility of the structure. Other solution is to coat the fiber with metal nanolayers to enable surface plasmon resonance excitation [13]. Although the sensitivities achieved with these sensors can be very high, the fabrication procedure is complex, and the very broad spectral resonances can increase the difficulty in the interrogation setup [12]. The sensitivity can also be enhanced by inserting the fluid inside the hollow structures of a microstructured optical fiber [14]. However, this is

#456529 https://doi.org/10.1364/OE.456529
Journal © 2022 Received 16 Feb 2022; revised 23 Mar 2022; accepted 24 Mar 2022; published 9 May 2022

Optics EXPRESS

a very challenging task, which not only requires stable setups, but also can have cleaning and contamination issues.

On the other hand, when a sensor is designed for the measurement of liquid refractive index, care must be taken to minimize cross-sensitivity to temperature. In many configurations, optical fiber sensors are inherently sensitive to temperature, which can require additional sensing elements to compensate these effects. Furthermore, as the temperature changes, it causes a change in the solution density, leading to a refractive index variation. Many works discuss only the sensor response to refractive index, without detailed analysis regarding the temperature influence. Other sensors were proposed to measure simultaneously both parameters, taking advantage of the different sensitivities attained for different sensing elements [4]. However, fewer devices have been developed to compensate the temperature effects, providing temperature independent refractive index values [15–18].

In this work, an inline sensor based on a hollow square core microstructured fiber section spliced between two SMFs is proposed. The sensor is used for simultaneous measurement of refractive index and temperature of glucose aqueous solutions, by resorting to a cladding modal interferometer and a Mach-Zehnder interferometer. It should be highlighted that each liquid sample surrounds the sensor, facilitating the measurement and cleaning procedures, and reducing the contamination issues. The different responses attained for both measurands allow a compensation of the temperature effects, attaining a refractive index detection that is temperature independent.

2. Operation principle

The guiding mechanism of the hollow square core fiber (HSCF) used in this work is based on antiresonance, as described in a previous work [19]. However, due to fiber inner geometry and the small core dimensions, other interferometric paths arise when a small section is spliced between two sections of single mode fiber (SMF). When the fiber is surrounded by liquid media, and the C + L band is used to interrogate the sensor, these interferometers become dominant over the antiresonance effects. Figure 1(a) shows a schematic design of the HSCF and Fig. 1(b) illustrates the different light propagation paths occurring in the proposed sensor.

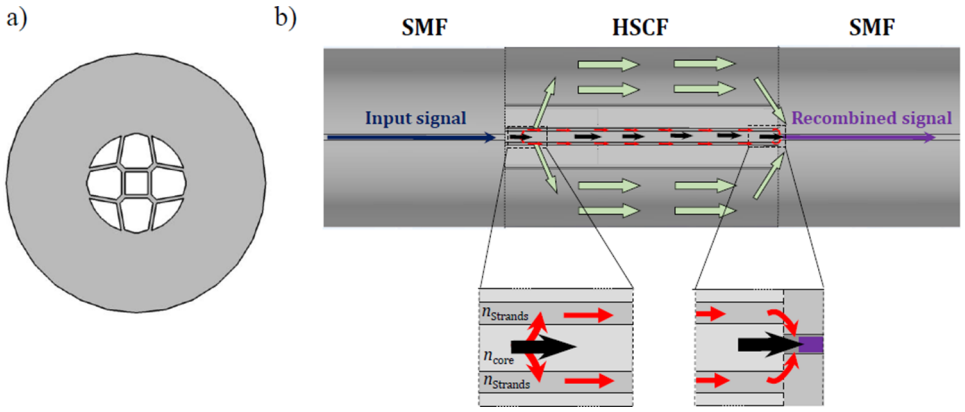

Fig. 1. Scheme of (a) the transverse profile of the HSCF and (b) the proposed sensor, with the different interferometric paths represented by arrows.

When the propagating mode of the SMF reaches the first interface between the SMF and HSCF, it will expand according to the numerical aperture, and different modes will be excited within the hollow core. Aside from these air propagating modes, there will also be coupling to the silica strands that surround the core (represented by the red arrows in Fig. 1(b). The modes

Optics EXPRESS

that propagate in the strands will experience a different medium than the core. This induces a phase shift between the core and strand modes so that when they couple back to the exit SMF their recombination will result in a Mach-Zehnder interference (MZI). This phase shift can be described as [20]:

$$\phi_{MZI} = 2\pi(n_{eff}^{strands} - n_{eff}^{core})L/\lambda_{MZI}, \tag{1}$$

where the $n_{eff}^{strands}$ and n_{eff}^{core} are the effective refractive indices of the modes propagating in the strands and core of the HSCF, respectively, L is the HSCF length and λ_{MZI} the operating wavelength. Furthermore, the output power resultant from this interference is given by [21]:

$$I_{MZI} = I_{core} + I_{strands} + 2\sqrt{I_{core}I_{strands}}cos\phi_{MZI}, \tag{2}$$

where I_{core} and $I_{strands}$ correspond to the intensity of the modes propagating in the core and strands, respectively. As this interferometer is formed in the inner part of the HSCF, there will be no interaction between the liquid sample and the sensing element, thus, an insensitivity towards external refractive index is expected.

On the other hand, some of the modes in the HSCF strands will be coupled to its outer cladding region (represented by the green arrows in Fig. 1(b)). The excited cladding modes, which present different propagating constants and different optical paths, will interfere between each other, generating a cladding modal interferometer (CMI). Considering, as first approximation, the interaction between two dominant modes, this interference will have maxima when the difference in the optical path is λ and minima when it is $\lambda/2$. Therefore, the CMI phase, ϕ_{CMI}, can be generally described as [20]:

$$\phi_{CMI} = 2\pi[n_{eff}^{cl,i}(\lambda) - n_{eff}^{cl,j}(\lambda)]\frac{L}{\lambda_{CMI}} = 2\pi m, \tag{3}$$

where $n_{eff}^{cl,i}(\lambda)$ and $n_{eff}^{cl,j}(\lambda)$ are the effective refractive indices of the i^{th} and j^{th} propagating cladding modes, and m is the order of resonance. Notice that, as this interferometer occurs within the cladding region, it is expected to be sensitive to the external refractive variations.

From Eqs. (1) and (3), it is possible to infer the free spectral range (FSR) of each interferometer i as being:

$$FSR^i = \frac{\lambda_1^i.\lambda_2^i}{L\Delta n_{eff}^i}, \tag{4}$$

where λ_1^i and λ_2^i are the wavelengths of two adjacent maxima, and Δn_{eff}^i is the difference between the two cladding modes effective refractive indices in the case of the CMI, or the difference between the effective refractive indices of the modes propagating in the strands and the core of the HSCF, for the case of the MZI.

3. Materials and methods

3.1. Sensor fabrication

The sensors were produced by splicing a section of the HSCF between two sections of single mode fiber (SMF28), following the details described elsewhere [19]. The fiber, whose cross section is shown in Fig. 2, presents a squared air core with side length of 11 µm, surrounded by thin silica strands with 1.7 µm of thickness, surrounded by thin silica strands with 1.7 µm of thickness. Between the core and the external silica cladding, there are hollow microstructures. Further details regarding the HSCF dimensions can be found in [19]. Several sensors were produced, with lengths ranging from 3.7 mm up to 16.0 mm. The length of each sensor was measured with a caliper.

Optics EXPRESS

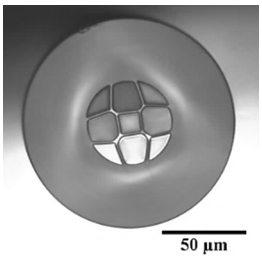

Fig. 2. Microscope photograph of the HSCF.

3.2. Experimental setup and spectral analysis

The sensor response was monitored in transmission, as shown in Fig. 3. The broadband optical source (Amonics ALS-CL-17-B-FA), centered at 1570 nm, has a bandwidth of 80 nm. The optical spectrum analyzer (OSA ANDO AQ6317C) was set to a resolution of 0.05 nm. To perform liquid refractive index measurements, the sensor was placed in a support structure, centered on a microscope slide, and throughout the experiments it was kept straight without tension applied, to minimize the optical losses due to fiber bending or strain. The liquid sample was placed in direct contact with the whole sensing structure. Between measurements, both the sensor and the microscope slide were cleaned with ethanol and dried at room temperature. The cleaning procedure took less than 2 minutes.

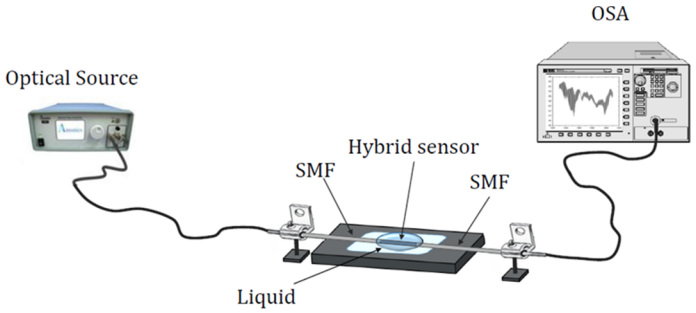

Fig. 3. Scheme of the experimental setup.

Figure 4 (left) presents the spectra attained for three sensors with the HSCF length ranging from 3.7 mm and 11.7 mm, with deionized water as surrounding medium. In all cases, there is a high frequency signal modulated by a lower frequency. Also in that Figure, the spectra obtained when the sensor is surrounded by index matching gel is presented. Notice that in this case, with the decrease of the refractive index difference at the external cladding/ surrounding medium interface, the CMI is no longer discernible. However, the MZI is clearly pronounced, together with a low frequency modulation. This corroborates with the argument that the MZI is formed in the inner region of the HSCF (hollow core and silica strands). This analysis can also be extended to the fast Fourier transform (FFT) obtained with water and index matching gel as surrounding media, also depicted in Fig. 4 (right), where three different regions can be distinguished. The first one, highlighted by the green rectangle, is probably due to the interference between modes propagating in the hollow core. This frequency remains unaltered and shows no sensitivity towards the parameters under study in this work. The second region, marked by the pink rectangle, corresponds to the CMI, whereas the higher frequencies, highlighted by the yellow rectangle, are due to the MZI. Notice that as the sensor length increases, the losses in

Optics EXPRESS

the MZI increase, diminishing the visibility of the high frequency. On the other hand, the CMI becomes more notorious. The sensor response was analyzed by employing adequate FFT filters. As the surrounding refractive index increases, the visibility of the lower frequency diminishes, whereas both the MZI and the lowest frequency (green rectangle) remain unaltered.

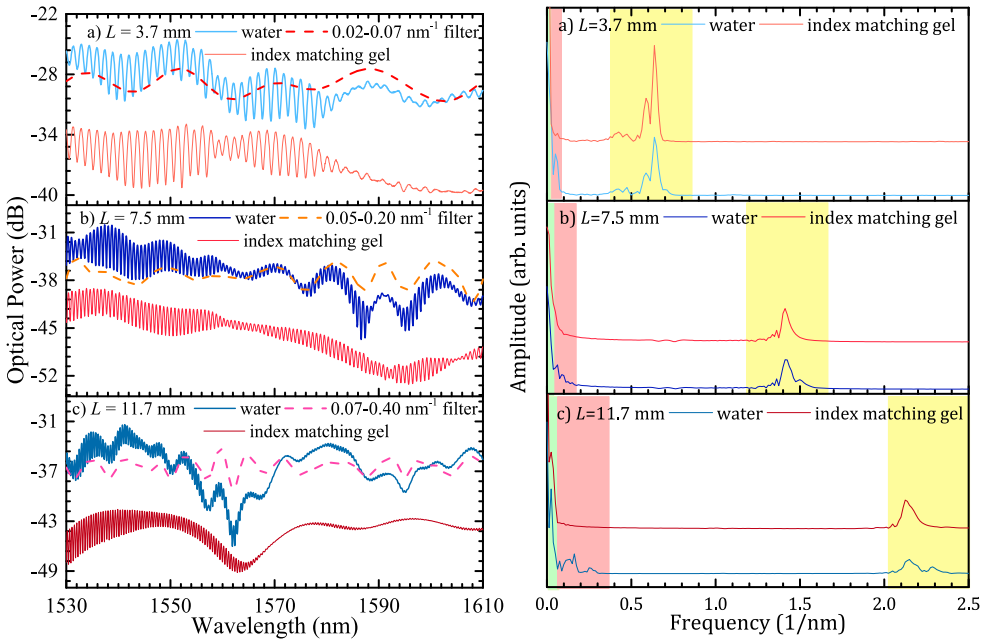

Fig. 4. (left) Transmission spectra for three sensors with different lengths, when surrounded by deionized water and index matching gel. The dashed lines represent the CMI bandpass filter. A shift in the optical power was done in the index matching gel spectra for ease of perception. (right) FFT for each sensor when the surrounding medium is water and index matching gel (with a shift in amplitude for ease of perception).

The effective refractive index of both interferometers was determined through the spectral analysis, considering FSR in each frequency region, as can be seen in Fig. 5. Both MZI and CMI peaks that were monitored were carefully chosen near the 1570 nm region. Notice that, in the case of the CMI, although several modes may be generated in the silica cladding region, only the interaction between two dominant modes is considered, as a first approximation. As expected, for both CMI and MZI, the longer the sensors, the smaller the FSR. The behaviors are well described by Eq. (4), where one considered that $\lambda_1^{CMI,MZI} \approx \lambda_2^{CMI,MZI}$ leading to $\lambda_1^{CMI,MZI} \cdot \lambda_2^{CMI,MZI} = \lambda^2$, with λ as 1570 nm (center wavelength). Also, the FSR was considered to be small enough to assume that the refractive index is independent of the wavelength. A fitting was done to the experimental values, attaining an effective refractive index of 0.042 and 0.388, respectively for the CMI and MZI, corroborating with the theoretical analysis.

3.3. Preparation of water-glucose solutions

A series of deionized glucose aqueous solutions were prepared under a controlled laboratory environment and stored for 24 h to allow their stabilization. The water was deionized in an in-house facility, and commercial glucose-D(+) anhydrous was used. The solutions had different weight percentages (wt.%) of glucose, starting at 0 wt.% up to 35 wt.%, in steps of 2.5 wt.%. After the stabilization period, the refractive index of each solution was measured using an Abbe refractometer (KRÜSS optronic refractometer) operating at 589 nm. The wt.% variation with the

Optics EXPRESS

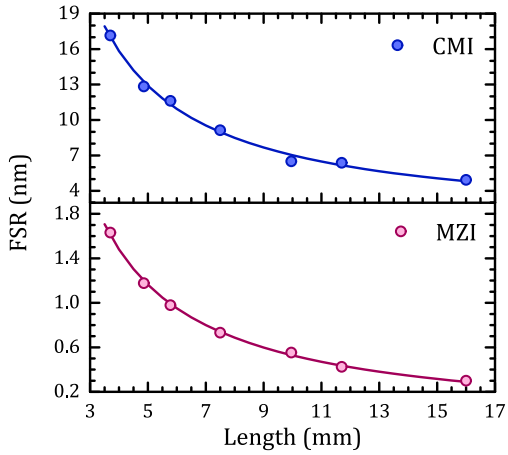

Fig. 5. Free spectral range dependence with the sensor length, for both interferometers under study. The reciprocal fitting $FSR = 1/(0.017\times10^{-6}\ L)$ and $FSR = 1/(0.158\times10^{-6}\ L)$ were attained for the CMI and MZI, respectively, where the FSR is in nm and the L is in mm.

measured refractive index, shown in Fig. 6, was approximated to a linear fitting, and the equation attained was $n_{589nm} = 1.640 \times 10^{-3} wt.\% + 1.330$ ($r^2 = 0.998$). It should be highlighted that these measurements were performed at room temperature (~20 °C), without compensating any temperature fluctuations. Since the fiber sensor operates in the 1550 nm region, a calibration procedure was carried out, using a multimode sensor based on a coreless fiber, combined with the method described in [10]. The refractive index dependence with wt.% at 1550 nm was determined to be $n_{1550nm} = 1.590\times10^{-3} wt.\% + 1.315$ ($r^2 = 0.995$).

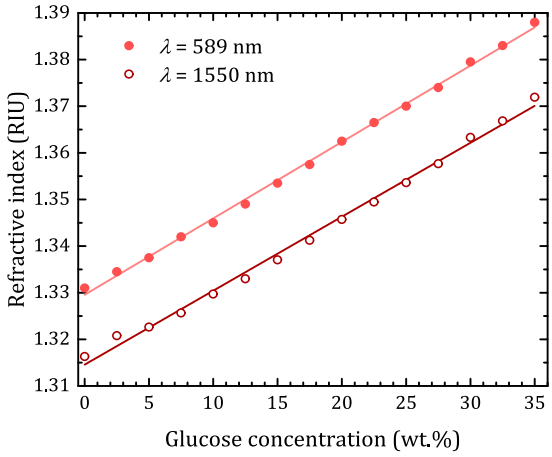

Fig. 6. Refractive index dependence with the glucose mass fraction, measured with the Abbe refractometer (@ 589 nm) and by an CMI sensor operating at 1550 nm.

4. Results and discussion

Figure 7(a) shows the spectral response of the 7.5 mm long sensor used in the experiments. The monitored MZI peak is highlighted in the inset. The filtered transmission spectrum of the sensor

Optics EXPRESS

used to attain the CMI component is presented in Fig. 7(b), together with the identification of the monitored CMI peak.

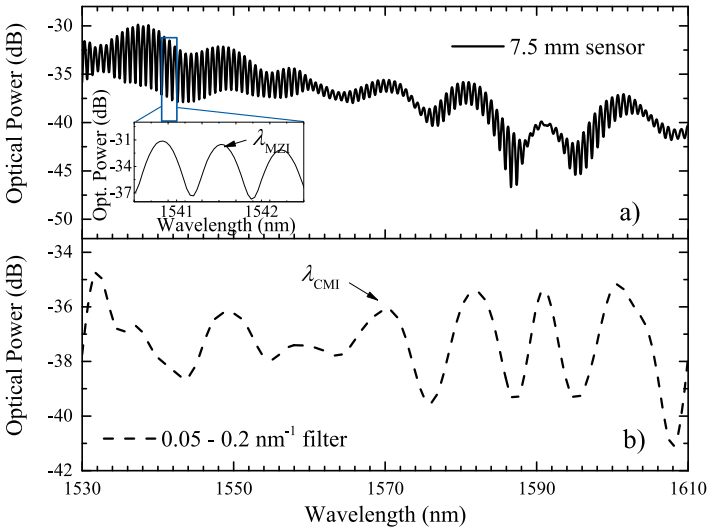

Fig. 7. (a) Spectral response of the 7.5 mm length sensor, with inset showing the MZI peak monitored. (b) Filtered spectrum used to monitor the CMI component.

Figure 8(a) shows the spectral response of the monitored MZI peak, while Fig. 8(b) shows the monitored CMI peak response, for glucose aqueous solutions with concentrations of 0, 2.5, and 5 wt.%. These components were monitored for all the glucose solutions. With this, the 7.5 mm long sensor response to the external refractive index variations, carried out at room temperature, allowed to attain two distinguishable behaviors, for the MZI and the CMI, as shown in Fig. 8(c)**.** The CMI presents a shift towards longer wavelengths (red shift), with a non-linear behavior, whereas the MZI shows no variation with the external refractive index, as expected. On the other hand, since the CMI occurs within the HSCF silica cladding, the evanescent field resultant of this interference is affected by variations of the external refractive index. The quadratic response is also justified since the interference wavelength is highly dependent on the evanescent field penetration depth, in turn, quadratically correlated with the refractive index of the external medium [10,22]. The CMI response was adjusted to the second order polynomial

$$\Delta\lambda_{MMI} = (9.4 \pm 6.5) \times 10^3 n^2 - (24.6 \pm 1.7) \times 10^3 n + (16.2 \pm 1.2) \times 10^3, \quad (5)$$

with a correlation factor of 0.9956. In order to compare this sensor with other devices already reported in the literature, it is useful to delimit two ranges where the response is considered approximate to a linear tendency. The first region, for lower refractive indices, comprises the variation between 1.315 and 1.348. The second region, for higher refractive indices, is between 1.348 and 1.371. A sensitivity of (318 ± 15) nm/RIU ($r^2 = 0.9823$) was attained for region 1, whereas for region 2 the sensitivity was of (922 ± 63) nm/RIU ($r^2 = 0.9773$). As the external refractive index increases, besides the CMI wavelength shift, there is also a decrease in the visibility of this component. For solutions with a concentration of glucose higher than 35 wt.%, the CMI response was no longer discernible, constituting the operation limit of the proposed sensor.

The sensor resolution was determined using deionized water and the 2.5 wt.% glucose aqueous solution. The wavelength shift was continuously monitored over a period of 15 minutes for each sample, with an acquisition rate of approximately 10 seconds (see Fig. 9). The respective

Optics EXPRESS

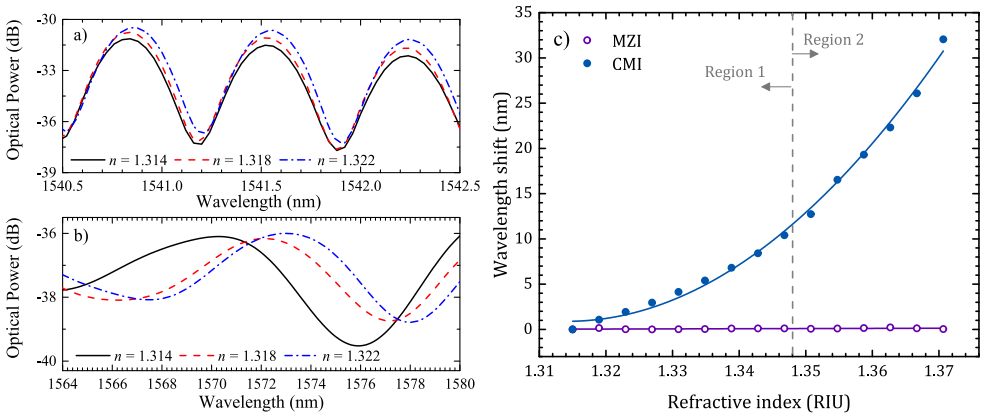

Fig. 8. Spectral responses of the (a) MZI and (b) CMI for three glucose aqueous solutions. (c) Sensor response with the refractive index variation, for both MZI and CMI. The two regions considered for the linearization are identified by the dashed line. For the first region the linear fitting equation is $\Delta\lambda$=(317.9 ± 15.1)n –(418.6 ± 20.1), and for the second region it is $\Delta\lambda$=(921.7 ± 62.7)n –(1232.7 ± 85.3).

minimum value of refractive index, δn, that this sensor can discern is given by [23]:

$$\delta n = 2\sigma_\lambda \Delta n/\Delta\lambda, \tag{6}$$

where σ_λ is the maximum wavelength standard deviation attained for both solutions, Δn is the variation of the refractive index, and $\Delta\lambda$ the mean wavelength shift. For the water sample, a mean wavelength of 1569.99 nm and a standard deviation of 7.1 pm were determined. For the 2.5 wt.% glucose, the mean wavelength was of 1570.98 nm, with a standard deviation of 12.5 pm. With this, a resolution of 1.0×10^{-4} was attained for the proposed sensor.

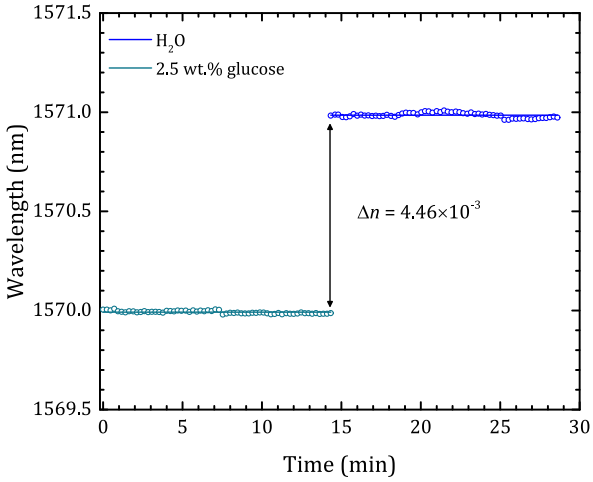

Fig. 9. Sensor response time to a refractive index step change to evaluate the system resolution.

To assess the sensor response to temperature variations within an aqueous environment, the sensor was inserted in a container with ~100 mL of liquid which was then subjected to temperature changes. A set of 8 glucose aqueous solutions with concentrations ranging from

Optics EXPRESS

0 up to 35 wt.% were used. A digital thermometer was placed near the HSCF to measure the liquid temperature. Care was taken so that the sensor was kept straight during the experiments. The temperature was changed from 25 °C up to 85 °C, in steps of 5 °C. Figure 10 presents the wavelength shift dependence with temperature, for both the MZI and CMI interferometers, and for solutions containing different wt.% of glucose. The linear response of the MZI to temperature variations is straightforwardly observed, with the interference wavelength presenting a variation towards longer wavelengths (redshift), whereas for the CMI the response is nonlinear with a shift towards shorter wavelengths (blueshift). Notice that the MZI response to temperature regarding the different concentrations of glucose solutions is similar, therefore presenting an identical sensitivity, whose mean fitting parameters are shown in Table 1. As the MZI is formed by two modes propagating in different media (silica and air), the difference in the effective refractive index gives rise to the sensitivity observed, translating in a dominance of the fiber thermo-optic coefficient over thermal expansion. The mean sensitivity attained, of (29.2 ± 1.1) pm/°C, is in good agreement with other MZIs reported in the literature [24–26].

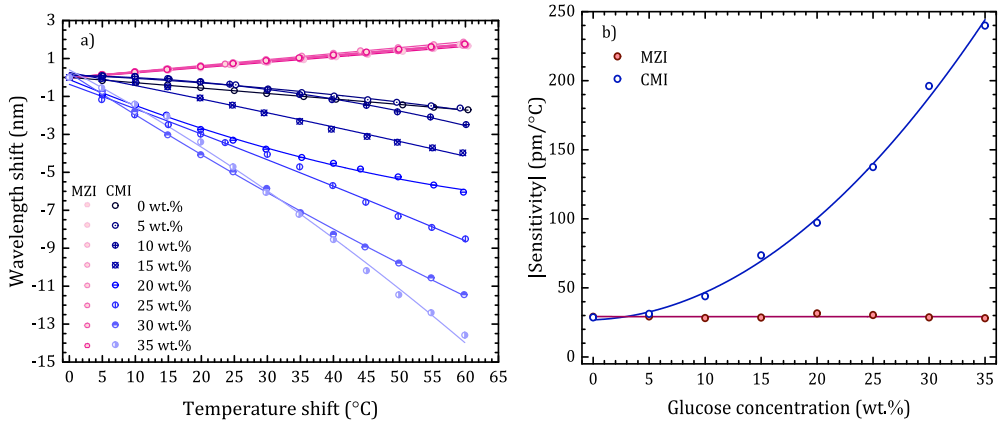

Fig. 10. (a) HSCF response to temperature shift of the MZI (pink dots) and CMI (blue dots) for the different glucose-water solutions. (b) Linear sensitivity dependence with glucose concentration for the MZI (solid pink dots) and for the CMI (hollow blue dots), where the curves are for ease of perception.

Table 1. Fitting parameters attained for the CMI at 25 °C, for the MZI component (mean values) and for the CMI for the different solutions tested. The MZI and CMI responses were adjusted to a linear fitting ($k_{T,MZI}T + k'_{T,MZI}$) and to a second order polynomial fitting ($k_{T,MMI}T^2 + k'_{T,MMI}T + k''_{T,MMI}$), respectively.

wt.% glucose	Fitting	r^2
0 - 35	$\lambda_{CMI}(n, T = (25°C) = (7.5 \pm 0.5) \times 10^3 n^2 - (19.5 \pm 1.4) \times 10^3 n + (14.2 \pm 0.9)$	0.9989
0 - 35	$\bar{\lambda}_{MZI}(T) = (29.2 \pm 1.1) \times 10^{-3} T + (1545.9 \pm 2.5)$	0.9994
0	$\lambda_{CMI}(T) = -(11.6 \pm 15.9) \times 10^{-6} T^2 - (27.4 \pm 1.8) \times 10^{-3} T + (1570.9 \pm 0.1)$	0.9990
5	$\lambda_{CMI}(T) = -(25.2 \pm 7.1) \times 10^{-5} T^2 - (3.5 \pm 7.9) \times 10^{-3} T + (1573.4 \pm 0.2)$	0.9840
10	$\lambda_{CMI}(T) = -(64.9 \pm 5.3) \times 10^{-5} T^2 - (27.8 \pm 5.9) \times 10^{-3} T + (1575.7 \pm 0.2)$	0.9955
15	$\lambda_{CMI}(T) = -(90.1 \pm 14.2) \times 10^{-6} T^2 - (63.6 \pm 15.8) \times 10^{-3} T + (1581.7 \pm 0.4)$	0.9880
20	$\lambda_{CMI}(T) = (78.5 \pm 9.1) \times 10^{-5} T^2 - (183.8 \pm 10.1) \times 10^{-3} T + (1589.9 \pm 0.3)$	0.9972
23	$\lambda_{CMI}(T) = -(16.5 \pm 21.1) \times 10^{-5} T^2 - (119.2 \pm 23.6) \times 10^{-3} T + (1591.6 \pm 0.6)$	0.9924
30	$\lambda_{CMI}(T) = (46.4 \pm 14.0) \times 10^{-5} T^2 - (247.3 \pm 15.6) \times 10^{-3} T + (1605.9 \pm 0.4)$	0.9983
35	$\lambda_{CMI}(T) = -(91.1 \pm 27.5) \times 10^{-5} T^2 - (139.1 \pm 30.8) \times 10^{-3} T + (1611.3 \pm 0.8)$	0.9957

Optics EXPRESS

In contrast, the CMI response suffers a more accentuated blueshift as the mass fraction of glucose increases. This is related to the liquid thermo-optic coefficient, which becomes larger for more concentrated samples. Although the CMI wavelength shift with temperature is non-linear, as a first approach, a linear fitting was applied. The estimated sensitivities, shown in Fig. 10 b), evidence the stability of the MZI response, when compared to the CMI. Notice that the CMI temperature sensitivity increases 8.4× between deionized water and 35 wt.% glucose. The second order fitting parameters that better describe the wavelength shift variation with temperature are shown in Fig. 10(a) are also presented in Table 1.

The wavelength variations measured for the water sample and shown in Fig. 10 a) were converted to refractive index variations through the linear fitting applied to the CMI in the first region (Fig. 8). With this, it was possible to estimate the thermo-optic coefficient of water as $(-1.13 \pm 0.02) \times 10^{-4}$ °C^{-1}, which is in good agreement with the values reported in the literature [27,28]. Thus, with this sensor it is also possible to estimate the thermo-optic coefficient of liquids, a matter that is out of the scope of this work.

Notice that the interference wavelength of the CMI depends both on refractive index and temperature variations, whereas the MZI is only mediated by temperature changes. The fitting parameters attained for a temperature of 25 °C are also shown in Table 1. The responses of the CMI and MZI, can be respectively described as:

$$\lambda_{CMI}(n,T) = k_{n1}n^2 + k'_{n1}n + k''_{n1} + k_{T1}T^2 + k'_{T1}T + k''_{T1}, \tag{7}$$

$$\lambda_{MZI}(T) = k_{T2}T + k'_{T2}, \tag{8}$$

where k_{n1}, k'_{n1} and k''_{n1} are the refractive index dependent coefficients estimated through the fittings, whereas $k_{T1,2}$, $k'_{T1,2}$ and k''_{T1} are the temperature dependent coefficients. A temperature compensation can be achieved by combining Eq. (7) and (8):

$$\lambda_{comp}(n) = \lambda_{CMI}(n,T) - k_{T1}\left(\frac{\lambda_{MZI}(T) - k'_{T2}}{k_{T2}}\right)^2 - k'_{T1}\left(\frac{\lambda_{MZI}(T) - k'_{T2}}{k_{T2}}\right) - k''_{T1}. \tag{9}$$

With this, it is possible to infer the temperature independent refractive index of each solution, by considering that the $\lambda_{comp}(n)$ is given by the first three terms on the right-hand side of Eq. (7), attaining:

$$n_{comp} = \frac{-k'_{n1} + \sqrt{k'^2_{n1} - 4k_{n1}.\left(k''_{n1} - \lambda_{comp}\right)}}{2k_{n1}}. \tag{10}$$

In Fig. 11, the CMI response to different glucose concentrations, without and with the temperature compensation is presented. Notice that after making the temperature compensation all the curves are superimposed, meaning that the wavelength variation is due only to variations on the glucose concentration. The same behavior is observed for the refractive index variation with glucose concentration, as shown in Fig. 12.

It is interesting to notice that the results shown in Fig. 12(b) were adjusted to a linear fitting, attaining a mean value of $n_{comp} = (1.57 \pm 0.04) \times 10^{-3} wt.\% + (1.315 \pm 0.005)$, which is in very good agreement with the fitted curve obtained during the calibration procedure.

A comparison between the proposed sensor sensitivity with the ones reported in the literature is presented in Table 2. Different strategies have been implemented by other research groups to improve the sensitivity to refractive index. For instance, the sensor diameter was decreased by means of chemical etching, or a thin metallic film was deposited on the fiber cladding. To make a fair comparison, only all silica-based sensors are considered in Table 2. Given the importance of the influence of temperature in this type of sensors, the comparison between the works regarding temperature compensation or simultaneous measurement of both parameters is also made.

Optics EXPRESS

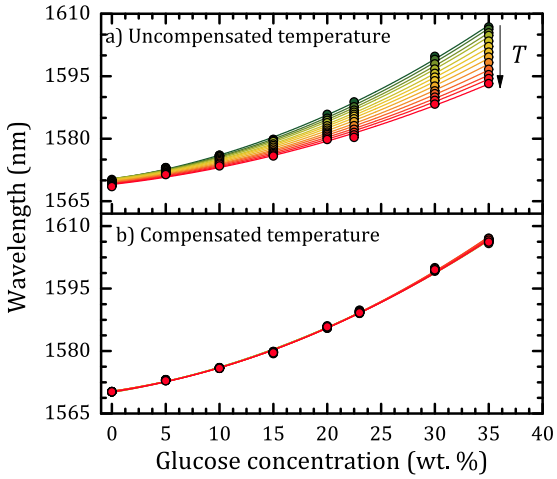

Fig. 11. Wavelength dependence on glucose concentration (a) without compensating temperature effects and (b) with temperature compensation.

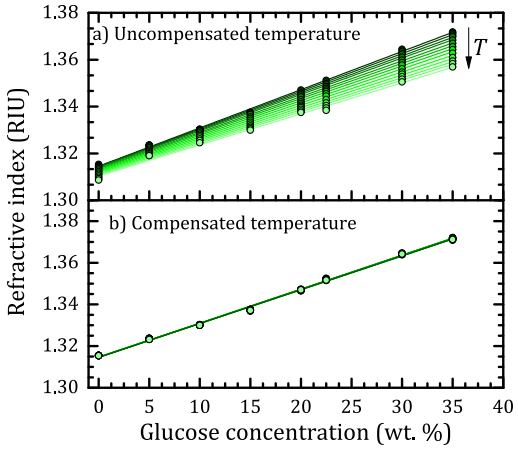

Fig. 12. Refractive index dependence on glucose concentration (a) without compensating temperature effects and (b) with temperature compensation.

Optics EXPRESS

Table 2. Sensing features based on all-silica based sensors and their refractive index sensitivity. Hi-Bi PMF is highly birefringent polarization maintaining fiber, CMF corresponds to coreless multimode fiber, and MCF is relative to multicore fiber. TC and SM stand for temperature compensation and simultaneous measurement, respectively.

Sensing structure			Range of operation (RIU)	Sensitivity (nm/RIU)	TC / SM?	Ref.
Configuration	Length (mm)	Diameter (μm)				
SMF + etched MMF	5	39	1.316–1.353 1.364–1.397	338.23 1012.66	no	[10]
SMF + etched MMF + SMF	23	40	1.33–1.3775	286.2	no	[11]
SMF + Hi-Bi PMF + CMF +SMF	280 + 52	125	1.336–1.344	90	SM	[12]
SMF + MMF + SMF + MMF + SMF	30	125	1.3105–1.3517	−37.9322	SM	[29]
SMF + ECF + SMF	3	200	1.41–1.43	890	no	[30]
Etched MCF	190	89	~1.44	47	TC	[31]
SMF + HSCF + SMF	7.5	125	1.330 - 1.348 1.348 - 1.371	318 ± 15 922 ± 63	TC	This work

5. Conclusion

A new optical fiber sensor based on a hollow square core fiber (HSCF) for the measurement of refractive index and temperature was proposed. Several sensing heads were developed, with varying lengths. Due to the HSCF inner geometry, it was possible to generate two different interferometers within the sensor, with different responses to both parameters under study. The cladding modal component revealed high sensitivity to the refractive index, comparable to other structures reported in the literature. With this sensor, a maximum sensitivity of (922 ± 63) nm/RIU was achieved for refractive index variations between 1.348 and 1.371. A temperature compensation method was also discussed. Furthermore, since the sensor outer diameter is similar to standard single mode fiber, the length is of only of a few millimeters, and the sample only surrounds the fiber, it becomes easier to handle, to clean, and low sample volumes are required for the experiments. In the context of an application, after a calibration of the sensor, it is possible to achieve a temperature independent measurement of refractive index. This can be particularly useful in applications where the control of the sample temperature is challenging, and the influence of this parameter needs to be mitigated. It should be highlighted that for samples with higher concentration of glucose this is particularly important, as the influence of temperature on the refractive index, through the thermo-optic effect, becomes more pronounced.

Funding. ; Bundesministerium für Bildung und Forschung (FKZ 03WKCV03E); Programa Operacional Regional do Centro (CENTRO-01-0145-FEDER-031568); Deutscher Akademischer Austauschdienst; Fundação para a Ciência e a Tecnologia (57518590, CEECIND/00777/2018, PTDC/EEI-EEE/31568/2017, UIDB/50025/2020, UIDP/50025/2020, BI/UI96/9133/2022).

Disclosures. The authors declare no conflicts of interest related to this article.

Data availability. Data underlying the results presented in this paper are not publicly available at this time but may be obtained from the authors upon reasonable request.

References

1. J. L. C. Perez, J. Gutiérrez- Gutiérrez, C. P. Mayoral, E. L. Pérez-Campos, M. S. P. Canseco, L. T. Carrillo, L. P. Mayoral, M. V. Treviño, E. L. Apreza, and R. R. Laguna, "Fiber optic sensors: a review for glucose measurement," Biosensors **11**(3), 61 (2021).
2. A. L. Galant, R. C. Kaufman, and J. D. Wilson, "Glucose: Detection and analysis," Food Chem. **188**, 149–160 (2015).

Optics EXPRESS

3. J. L. Santos and F. Farahi, *Handbook of optical sensors*, (CRC Press, Boca Raton, 2014), Chap.1.
4. A. Urrutia, I. Del Villar, P. Zubiate, and C. R. Zamarreño, "A comprehensive review of optical fiber refractometers: Toward a standard comparative criterion," Laser Photonics Rev. **13**(11), 1900094 (2019).
5. H. Tsuda and K. Urabe, "Characterization of long-period grating refractive index sensors and their applications," Sensors **9**(6), 4559–4571 (2009).
6. J. K. Sahota, N. Gupta, and D. Dhawan, "Fiber Bragg grating sensors for monitoring of physical parameters: a comprehensive review," Opt. Eng. **59**(6), 060901 (2020).
7. O. Rodríguez-Quiroz, C. E. Domínguez-Flores, D. Monzón-Hernández, and C. Moreno-Hernández, "Hybrid fiber Fabry–Perot interferometer with improved refractometric response," J. Lightwave Technol. **37**(17), 4268–4274 (2019).
8. Z. Li, Y. Wang, C. Liao, S. Liu, J. Zhou, X. Zhong, Y. Liu, K. Yang, Q. Wang, and G. Yin, "Temperature-insensitive refractive index sensor based on in-fiber Michelson interferometer," Sens. Actuators B: Chem. **199**, 31–35 (2014).
9. Q. Wang, L. Kong, Y. Dang, F. Xia, Y. Zhang, Y. Zhao, H. Hu, and J. Li, "High sensitivity refractive index sensor based on splicing points tapered SMF-PCF-SMF structure Mach-Zehnder mode interferometer," Sens. Actuators B: Chem. **225**, 213–220 (2016).
10. S. Novais, C. I. A. Ferreira, M. S. Ferreira, and J. L. Pinto, "Optical fiber tip for the measurement of glucose aqueous solutions," IEEE Photonics J. **10**(5), 1–9 (2018).
11. Y. Zhao, L. Cai, X. Li, F. Meng, and Z. Zhao, "Investigation of the high sensitivity RI sensor based on SMS fiber structure," Sens. Actuators A: Phys. **205**, 186–190 (2014).
12. C. Gouveia, G. Chesini, C. M. B. Cordeiro, J. M. Baptista, and P. A. S. Jorge, "Simultaneous measurement of refractive index and temperature using multimode interference inside a high birefringence fiber loop mirror," Sens. Actuators B: Chem. **177**, 717–723 (2013).
13. Y. Zhang, M. Liu, Y. Zhang, Z. Liu, X. Yang, J. Zhang, J. Yang, and L. Yuan, "Simultaneous measurement of temperature and refractive index based on a hybrid surface plasmon resonance multimode interference fiber sensor," Appl. Opt. **59**(4), 1225–1229 (2020).
14. J. Yang, C. Guan, P. Tian, T. Yuan, Z. Zhu, P. Li, J. Shi, J. Yang, and L. Yuan, "In-fiber refractive index sensor based on single eccentric hole-assisted dual-core fiber," Opt. Lett. **42**(21), 4470–4473 (2017).
15. S. Pevec and D. Donlagic, "High resolution, all-fiber, micro-machined sensor for simultaneous measurement of refractive index and temperature," Opt. Express **22**(13), 16241–16253 (2014).
16. A. Iadicicco, S. Campopiano, A. Cutolo, M. Giordano, and A. Cusano, "Self-temperature referenced refractive index sensor by non-uniform thinned fiber Bragg gratings," Sens. Actuators B: Chem. **120**(1), 231–237 (2006).
17. V. I. Ruiz-Perez, P. M. Velasco-Bolom, D. A. May-Arrioja, and J. R. G. Sepúlveda, "Measuring the thermo-optic coefficient of liquids with athermal multimode interference devices," IEEE Sens. J. **21**(3), 3004–3012 (2021).
18. J. Harris, P. Lu, H. Larocque, L. Chen, and X. Bao, "In-fiber Mach–Zehnder interferometric refractive index sensors with guided and leaky modes," Sens. Actuators B: Chem. **206**, 246–251 (2015).
19. D. Pereira, J. Bierlich, J. Kobelke, and M. S. Ferreira, "Double antiresonance fiber sensor for the simultaneous measurement of curvature and temperature," Sensors **21**(23), 7778 (2021).
20. W. Sun, X. Zhang, Y. Yu, L. Yang, F. Hou, Y. Yang, and T. Yang, "Comparative study on transmission mechanisms in a SMF-Capillary-SMF structure," J. Lightwave Technol. **38**(15), 1 (2020).
21. J. Liou and C. Yu, "All-fiber Mach-Zehnder interferometer based on two liquid infiltrations in a photonic crystal fiber," Opt. Express **23**(5), 6946–6951 (2015).
22. S. Silva, E. G. P. Pachon, M. A. R. Franco, J. G. Hayashi, F. X. Malcata, O. Frazão, P. Jorge, and C. M. B. Cordeiro, "Ultrahigh-sensitivity temperature fiber sensor based on multimode interference," Appl. Opt. **51**(16), 3236–3242 (2012).
23. R. Romero, O. Frazão, D. A. Pereira, H. M. Salgado, F. M. Araújo, and L. A. Ferreira, "Intensity-referenced and temperature-independent curvature-sensing concept based on chirped fiber Bragg gratings," Appl. Opt. **44**(18), 3821–3826 (2005).
24. S. Silva, O. Frazão, J. L. Santos, J. Kobelke, and K. Schuster, "Simultaneous measurement of three parameters using an all-fiber Mach-Zehnder interferometer based on suspended twin-core fibers," Opt. Eng. **50**(3), 030501 (2011).
25. C. E. S. Castellani, H. C. B. Ximenes, R. L. Silva, A. Frizera-Neto, M. R. N. Ribeiro, and M. J. Pontes, "Multi-parameter interferometric sensor based on a reduced diameter core axial offseted fiber," IEEE Photonics Technol. Lett. **29**(2), 239–242 (2017).
26. Y. Wang, Y. Zhou, Z. Liu, D. Chen, C. Lu, and H. Tam, "Sensitive Mach-Zehnder interferometric sensor based on a grapefruit microstructured fiber by lateral offset splicing," Opt. Express **28**(18), 26564–26571 (2020).
27. S. Novais, M. S. Ferreira, and J. L. Pinto, "Determination of thermo-optic coefficient of ethanol-water mixtures with optical fiber tip sensor," Opt. Fiber Technol. **45**, 276–279 (2018).
28. C. Lee, Y. Lu, C. Chen, and C. Ma, "Microhole-pair hollow core fiber Fabry–Perot interferometer micromachining by a femtosecond laser," Sens. Actuators A: Phys. **302**, 111798 (2020).
29. R. Xiong, H. Meng, Q. Yao, B. Huang, Y. Liu, and H. Xue, "simultaneous measurement of refractive index and temperature based on modal interference," IEEE Sens. J. **14**(8), 2524–2528 (2014).
30. J. H. Osório, W. M. Guimarães, L. Peng, M. A. R. Franco, S. C. Warren-Smith, H. Ebendorff-Heidepriem, and C. M. B. Cordeiro, "Exposed-core fiber multimode interference sensor," Results in Optics **5**, 100125 (2021).
31. Z. Zhu, D. Ba, L. Liu, L. Qiu, and Y. Dong, "Temperature-compensated distributed refractive index sensor based on an etched multi-core fiber in optical frequency domain reflectometry," Opt. Lett. **46**(17), 4308–4311 (2021).